Galvanic Brain-Coupled Communication Among Freely Floating Micro-Scale Implants

Matteo Pola*†, Vasiliki Giagka*§, Wouter A. Serdijn*, Danilo Demarchi†, Amin Rashidi*‡

*Bioelectronics Section, Dept. of Microelectronics, Delft University of Technology, Delft, The Netherlands
†Dept. of Electronics and Telecommunications, Politecnico di Torino, Turin, Italy
§ Fraunhofer Institute for Reliability and Microintegration IZM, Berlin, Germany
‡ imec The Netherlands, Eindhoven
Email: matteo.pola@studenti.polito.it, a.rashidi@ieee.org

Abstract—This paper presents a new communication method between micro-scale freely floating brain implants based on galvanic coupling (GC), called "Brain-Coupled Communication" (BCC). Since the transmission efficiency based on GC is highly dependent on the system's geometry and the electromagnetic properties of the tissue, finite element models in COMSOL Multiphysics® are employed for characterizing the proposed method. Concurrent scaling of channel length (i.e., the distance between two implants), the inter-electrode distance (on a single implant), and electrode dimensions with a constant ratio down to 2 % of their typical values show an increase in the optimum frequency of the communication by 50 times (from 200 kHz to 10 MHz). This, in turn, yields a substantial increase in the channel bandwidth. The proposed method also shows excellent robustness against misalignment. Up to 60 ° of angular misalignment and 1 mm of lateral displacement result in a voltage-gain attenuation of less than 5 dB and 2 dB, respectively. Furthermore, a negligible shading effect between implants is observed by exploring multi-implant scenarios. Moreover, based on the conducted compliance study, no safety hazards were observed for the intended conditions. In conclusion, the proposed method exhibits a multitude of desirable qualities that position it as an excellent choice for establishing a network of freely floating brain implants.

Index Terms—Micro-scale brain implants, Distributed neural interface, Human body communication, Galvanic coupling

I. Introduction

Brain-Computer Interface (BCI) platforms have received growing attention in the last decades, as an effective means of restoring sensory and motor functions (e.g. sight, movement, and cognitive abilities), in addition to their utility in neuroscience studies. Developing technologies to enable distributed neural interfaces for BCI systems is an active area of research aimed at optimizing scalability in the number of neural interfaces, expanding coverage to larger brain areas, and minimizing invasiveness through device miniaturization [1]. To this end, both wired solutions (e.g. the Neuralink project [2]), and wireless networks of miniaturized implants (e.g Neural Dust [3], Microbead [4], Neurograin [5], ENGINI [6], and STARDUST [7] projects) have been proposed in the literature [8]. The main advantage introduced by the distributed neural interfaces is the lower invasiveness of implants when a wide coverage of brain areas is required by the application [9].
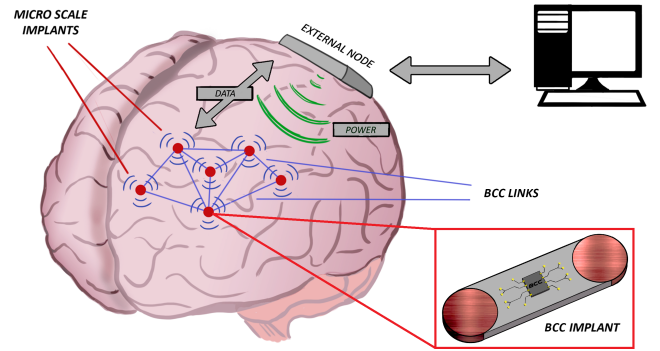
Fig. 1: Scheme of a completely wireless distributed BCI, with a zoom of a hypothetical BCC device design

Most wireless solutions utilize electromagnetic radiation for communications between implants and an external node. Alternatively, Human Body Communication (HBC) is a promising wireless technology that intrinsically offers lower power consumption, higher efficiency, low interference, and higher security compared to RF ("radio-frequency") solutions [10]. HBC is based on coupling coils or metallic electrodes directly to the human tissues to transmit non-radiative signals through the body itself, working in the reactive near-field region. Without the need for an antenna to create electromagnetic radiation, the transmitting frequency can be lowered with no constraints in terms of the dimension of the device. HBC can be achieved with three types of coupling: capacitive, galvanic, and magnetic. While capacitive HBC is more suitable for larger distances, the galvanic coupling is typically preferred for implants due to its independence from the environment and earth ground, higher security, and privacy of the propagated signals [11]–[14]. Banou et al. [13] focused on galvanic HBC implants with a collision-free protocol and near-field beamforming. Noormohammadi et al. [14] demonstrated successful galvanic HBC in the in-body-to-on-body scenario, using a baseband impulse technique without a high-frequency carrier.

In this work, we are proposing brain-coupled for communication between micro-scale implants based on galvanic coupling, as depicted in Fig. 1. We study, for the first time, the effect of scaling the communication channel to a micro-scale level. Furthermore, we explore the misalignment effect and multi-
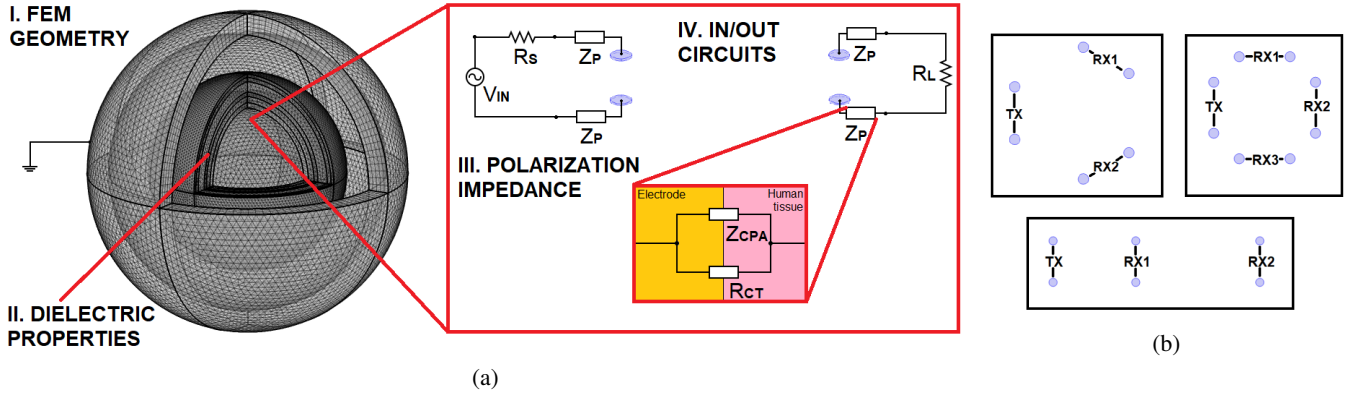
Fig. 2: a) Scheme of the complete model with highlights of the main feature and b) configurations of small networks to study the shadowing effect between receivers
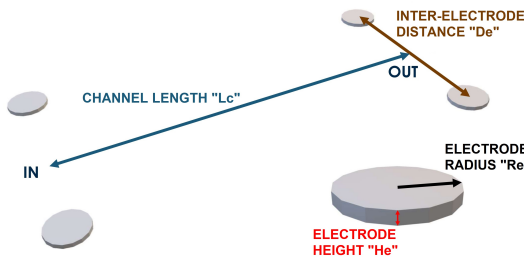

Fig. 3: Highlight on the geometrical parameters of two devices

device configurations. The simulation results provide valuable insights into the potential of galvanic coupling for communication between micro-scale implants and highlight important design considerations for their future development.

II. METHODOLOGY

This study builds on state-of-the-art research on galvanic coupling for implants [15], [16], [17] by developing a FEM (Finite Element Method) model in COMSOL Multiphysics® 6.0. The model is designed to simulate different scenarios, in which micro-scale brain implants communicate through galvanic coupling. To this end, a frequency-domain study was conducted using two *AC/DC Module* interfaces: *Electric Currents* and *Electrical Circuits*. The former exploits the quasi-static approximation to solve the electrical potential in any point of the geometry, and the latter allows for the coupling of ideal electronic circuits to the FEM model. The final simulation setup depicted in Fig.2(a) is obtained through the following steps:

STEP I - GEOMETRY: The human head is modeled by a layered sphere containing the main tissues in the human head (from the outermost to the innermost): skin, fat, bone, dura mater, cerebrospinal fluid (CSF), gray matter, and white matter, surrounded by an infinite unbounded air domain. Then, two couples of platinum cylinders, each representing the two electrodes of the transmitting/receiving implant, are placed into the innermost layer of the sphere, i.e. the white matter (Fig. 2(a.I)).

STEP II - DIELECTRIC CHARACTERISTICS: For the targeted simulations, the dielectric properties of the materials, i.e. the relative permittivity (ϵ_r) and the electrical conductivity (σ), are required to solve the Maxwell equations, which are simplified by the quasi-static approximation. Inside the sphere, each layer was described with the proper ϵ_r and σ, according to the parametric Cole-Cole model of the complex permittivity ϵ^* [18]. The frequency-dependent dielectric characteristics are imported to the model from [19].

STEP III - POLARIZATION IMPEDANCE: The electrical double layer describes the disposition of charges at the metal-tissue interface, where Faradaic and non-Faradaic processes arise. To take this phenomenon into account, it is necessary to define a polarization impedance Z_P (Fig. 2(a.III)), composed of a pseudo-capacitance with constant phase angle Z_{CPA} and a charge-transfer resistance R_{CT} in parallel as described in [20]. Then, Z_P is included in the FEM model with a surface impedance on the outside of each cylinder using the *Distributed Impedance* function in the *Electric Currents* module.

STEP IV - EQUIVALENT CIRCUITS: The two electrodes of each device are linked to simplified equivalent circuits representing the transmitter and the receiver. The circuits include a sinusoidal source and two resistors, arranged as shown in Fig. 2(a.IV), and their default values are 1 V and 50 Ω, respectively. Through the circuits, it was also possible to define a different ground for each side, preventing the common-ground effect.

STEP V - FREQUENCY DOMAIN STUDY: To complete the simulation setup, the *Extremely fine* mesh is selected due to the small dimension of the electrodes, and the outermost surface of the air domain is fixed to ground to ensure the convergence of the solution. A frequency-domain study is conducted within (10 kHz-1 GHz) to obtain the frequency response in the galvanic coupling communication channel.

Once the model has been completed, it is used to examine the effects of various parameters on the communication's transfer function. The analyzed parameters are illustrated in Fig. 3, and include the electrode radius ("R_e"), the electrode height
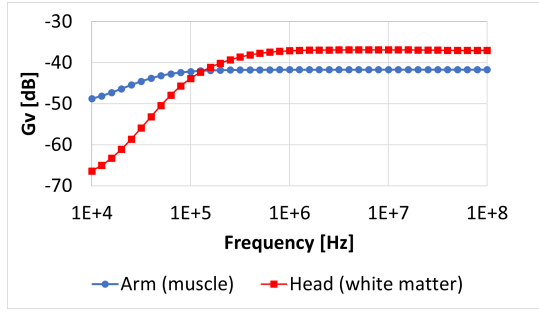
Fig. 4: Voltage gain in muscle [16] and white matter

(”H_e”), the inter-electrode distance in the implants (”D_e”), the channel length (”L_c”, the distance between two implants). Furthermore, the effect of angular and spatial misalignments, the location of the implant (white or gray matter), as well as the generator's internal resistance (”R_S”), and the load resistance (”R_L”) are explored. Finally, multi-implant scenarios (see Fig. 2(b)) and compliance with the ICNIRP (”International Commission On Non-Ionizing Radiation Protection”) safety regulations are studied.

III. RESULTS

The main parameter used to evaluate the results of the simulations is the voltage gain, G_V, which is calculated as $20 \log_{10} |V_R/V_T|$, where V_R and V_T represent the differential voltages at the receiver and transmitter electrodes, respectively. V_R itself was observed as well, in order to study the sensitivity required at the receiver side.

The first simulation compares the model of this work with the one in [16], keeping the same dimensions of the electrodes as the latter (D_e=5 cm, L_c=10 cm, R_e=5 mm, and H_e=1 mm), to study the impact of different tissue material, i.e. the brain's white matter versus the muscle tissues, on G_V. The curves obtained (see Fig. 4) have the same high-pass behavior, but the peak is higher in the case of white matter (-37 dB vs -42 dB), while the cut-off frequency is lower in the muscle (30 kHz vs 200 kHz). Similar simulations in gray matter show around 1 dB improvement in the peak value. Hereafter, all the results are presented for the brain's white matter.

In the next step, D_e, L_c, R_e, and H_e are scaled concurrently and with a constant scaling factor (k), to investigate the effect of system scaling on the transfer function of G_V, and peak value of V_R. The results show that a proportional decrease of D_e from 5 cm to 1 mm, results in a reduction of the peak of G_V from around -37 dB to -47 dB (Fig. 5(a)). However, as shown in Fig. 5(b), the peak frequency of V_R, which is around the cut-off frequency of G_V, increases as the channel geometry scales to smaller dimensions, making it more suitable for high data-rate communications. For example, when using a data carrier frequency of 10 MHz, the amplitude of V_R increases from 0.3 mV for k=1 to approximately 2 mV for k=0.02 (Fig. 5(c)). This substantial increase in V_R results in 7 times lower sensitivity required at the receiver. For the highest explored scaling factor (i.e. R_e=0.1 mm, and H_e=0.02

mm), varying L_c from 2 mm to 5 cm with D_e=1 mm leads to the decrease in the peak of G_V from -47 dB to -120 dB (Fig. 6(a)). Varying D_e in the range from 0.5 mm to 2 mm with L_c=5 mm, results in G_V's peak rising from -81 dB to -59 dB (Fig. 6(b)). The two behaviors are in line with the previous findings about galvanic coupling [15], [16], where the intensity of the electric fields is inversely proportional to the distance from the source, and a higher current density is spread to a bigger portion of tissue when the transmitting electrodes are further away from each other. Additionally, the proposed BCC method demonstrates good robustness in multi-implant scenarios and against misalignment. Angular misalignment of up to 60° and a lateral displacement of up to 1 mm result in a G_V attenuation of less than 5 dB and 2 dB, respectively. Fig. 6(c) shows the results on G_V for both in-plane and out-of-plane angular misalignments of the receiving electrodes. Furthermore, according to the simulations with more than two devices as in Fig. 2(b), no shadowing effect is observed between the devices and only slight variations in G_V appear when the devices share the same current flow. This could be expected as the current flow only depends on the path where the minimum resistance is encountered. Moreover, the impact of different electrode materials as well as source and load resistors on the peak value of G_V is investigated. Using copper instead of platinum electrodes shows negligible impact on the results. To study the impact of source and load resistances, R_S and R_L are swept from 20 Ω to 1 kΩ and from 50 Ω to 1 MΩ, respectively, instead of their default 50 Ω value. While the change in R_S has a negligible impact on G_V, increasing R_L allows for a flattening of the transfer function within the observed frequency range, resulting in a shift of the cut-off frequency to lower values.

In this section, compliance with the ICNIRP2020 safety regulations [21] is explored for the highest-scaled scenario (k=0.02). So-called "basic restrictions" in [21] define the main quantities that restrict electromagnetic fields induced inside the human body. They include the spacial Root Mean Square (RMS) of the electric field in a 2 mm x 2 mm x 2 mm box (E_{ind}) and the spatial RMS of the Specific Absorption Rate in 10 g of contiguous tissue (SAR_{10g}). The former prevents the unwanted electrostimulation of the nerves and the latter the thermal effects that can arise and damage the tissues. Fig. 7(a & b) show the values of E_{ind} and SAR_{10g} calculated around the transmitting electrodes in the model for varying input signal amplitudes from 0.3 V to 1 V, together with their basic restrictions. It is possible to notice that the electric field regulations are met for frequencies above 1 MHz, while the maximum SAR is respected across the entire frequency range. Lastly, it is essential to discuss the limitations of the model. The definitions of the reactive near-field region and the quasi-static approximation are based on the relationship between a specific length in the model and the wavelength (λ) in the medium, which, in this case, is the white matter. To operate within the reactive near-field, the distance from the source, including the channel length, must be significantly smaller than $\lambda/2\pi$. Similarly, to apply the quasi-static approximation,
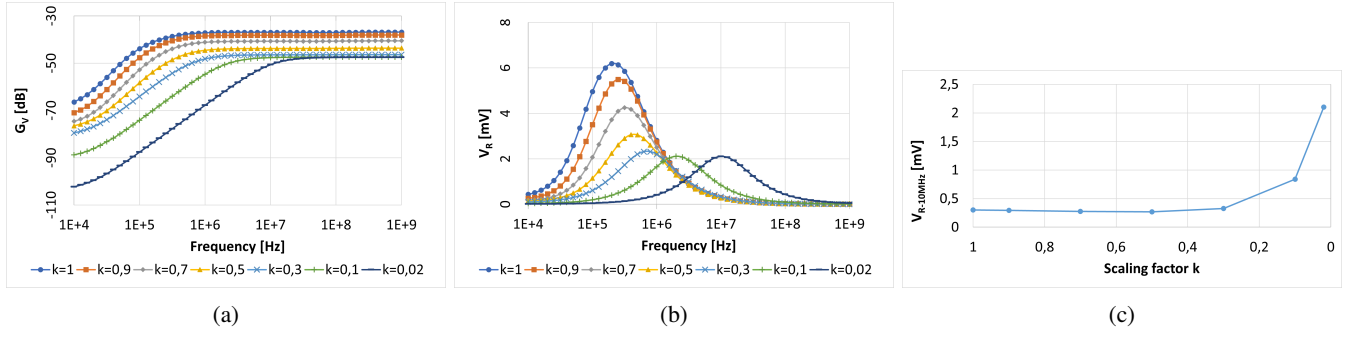
Fig. 5: a) Voltage gain, b) received voltage and c) focus on its value at 10 MHz, all for different scaling factors
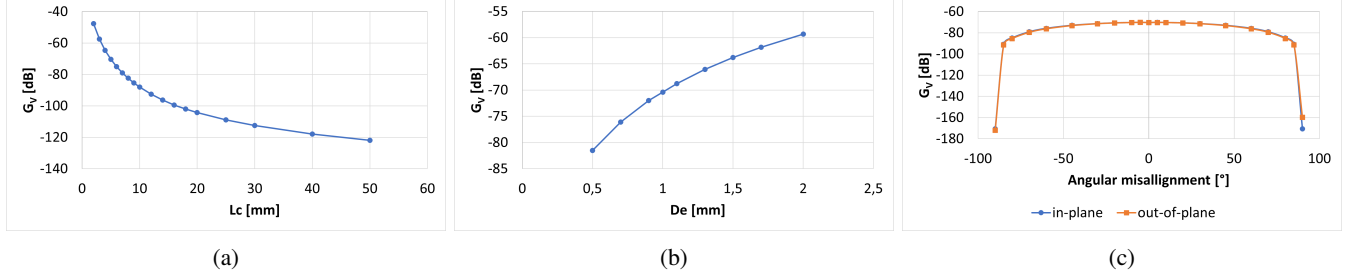

Fig. 6: Voltage gain peak for different a) channel lengths, b) inter-electrode distances, and c) angular misalignments
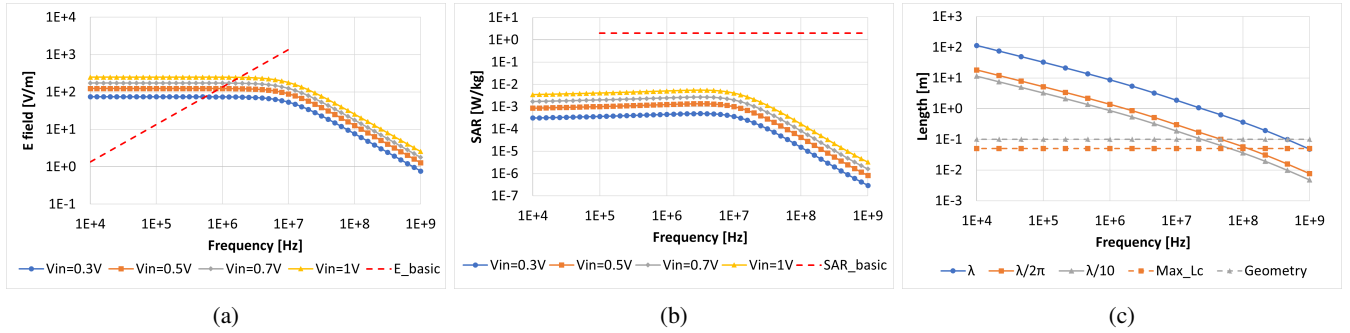

Fig. 7: a) Average electric field and b) SAR for different input signal amplitude with related basic restrictions from [21], and c) model validity limits related to reactive near-field zone and quasi-static approximation

the geometry must be considerably smaller than λ, typically less than $\lambda/10$. In Fig. 7(c) the values of λ, $\lambda/2\pi$, and $\lambda/10$ are plotted together with the maximum dimensions used in the simulations, 5 cm and 10 cm for channel length and geometry, respectively. As a result, the requirements of non-radiative fields and the quasi-static analysis hold valid up to 25 MHz and 100 MHz. Exceeding this limit can lead to radiation outside the body, with consequent losses in the transmission, and non-negligible errors in the simulations. For an electrode diameter of 200 µm, the highest gain can be achieved at frequencies around 10 MHz, which still has a good margin to the model's validity limit.

IV. CONCLUSIONS

This paper presents a detailed study of adopting galvanic coupling for a network of wireless free-floating brain implants, using FEM simulations. The study involves the construction of a layered sphere model, representing the human head, and pairs of platinum electrodes, representing the implants, using COMSOL Multiphysics®. Various factors, including electrode geometry, channel length, misalignments (both angular and spatial), and source/load resistances are examined for their impact on the voltage gain between the transmitting and receiving electrodes (G_V). The simulations show that proportional scaling of the channel and electrode dimensions toward micro-scale implants degrades the absolute peak of G_V, necessitating higher sensitivity at the receiver side. At the same time, the peak of the received voltage moves to higher frequencies, allowing for an improvement in the data rate. The communication channel shows great robustness against different misalignments and shadowing by other implants, making it suitable for freely floating micro-scale implants in the brain. Finally, compliance with safety regulations is explored which shows no safety hazard for the targeted operating frequencies.

REFERENCES

[1] K. M. Szostak, P. Feng, F. Mazza, and T. G. Constandinou, *Distributed neural interfaces: challenges and trends in scaling implantable technology.* Singapore: Springer Singapore, 2020, pp. 1–37.

[2] E. Musk and Neuralink, "An integrated brain-machine interface platform with thousands of channels," *Journal of Medical Internet Research*, vol. 21, 10 2019.

[3] D. Seo, J. M. Carmena, J. M. Rabaey, E. Alon, and M. M. Maharbiz, "Neural dust: an ultrasonic, low power solution for chronic brain-machine interfaces," 7 2013.

[4] A. Khalifa, Y. Liu, Y. Karimi, Q. Wang, A. Eisape, M. Stanaćević, N. Thakor, Z. Bao, and R. Etienne-Cummings, "The microbead: a 0.009 mm3 implantable wireless neural stimulator," *IEEE Transactions on Biomedical Circuits and Systems*, vol. 13, pp. 971–985, 10 2019.

[5] J. Lee, V. Leung, A. H. Lee, J. Huang, P. Asbeck, P. P. Mercier, S. Shellhammer, L. Larson, F. Laiwalla, and A. Nurmikko, "Neural recording and stimulation using wireless networks of microimplants," *Nature Electronics*, vol. 4, pp. 604–614, 8 2021.

[6] N. Ahmadi, M. L. Cavuto, P. Feng, L. B. Leene, M. Maslik, F. Mazza, O. Savolainen, K. M. Szostak, C.-S. Bouganis, J. Ekanayake, A. Jackson, and T. G. Constandinou, "Towards a distributed, chronically-implantable neural interface," 2019.

[7] A. Rashidi, S. Hosseini, K. Laursen, and F. Moradi, "Stardust: Optogenetics, electrophysiology and pharmacology with an ultrasonically powered dust for parkinson's disease," in *2019 26th IEEE International Conference on Electronics, Circuits and Systems (ICECS)*. IEEE, 2019, pp. 109–110.

[8] Y. Liu, A. Urso, R. M. D. Ponte, T. Costa, V. Valente, V. Giagka, W. A. Serdijn, T. G. Constandinou, and T. Denison, "Bidirectional bioelectronic interfaces: System design and circuit implications," *IEEE Solid-State Circuits Magazine*, vol. 12, pp. 30–46, 3 2020.

[9] D. De Ridder, J. Maciaczyk, and S. Vanneste, "The future of neuromodulation: Smart neuromodulation," *Expert Review of Medical Devices*, vol. 18, no. 4, pp. 307–317, 2021.

[10] T. G. Zimmerman and S. A. Benton, "Personal area networks (pan): Near-field intra-body communication," 1995.

[11] M. S. Wegmüller, "Intra-body communication for biomedical sensor networks," 2007.

[12] J. Jang, J. Lee, K. R. Lee, J. Lee, M. Kim, Y. Lee, J. Bae, and H. J. Yoo, "A four-camera vga-resolution capsule endoscope system with 80-mb/s body channel communication transceiver and sub-centimeter range capsule localization," *IEEE Journal of Solid-State Circuits*, vol. 54, pp. 538–549, 2 2019.

[13] S. Banou, M. Swaminathan, G. R. Muns, D. Duong, F. Kulsoom, P. Savazzi, A. Vizziello, and K. R. Chowdhury, "Beamforming galvanic coupling signals for iomt implant-to-relay communication," *IEEE Sensors Journal*, vol. 19, pp. 8487–8501, 10 2019.

[14] R. Noormohammadi, A. Khaleghi, and I. Balasingham, "Galvanic impulse wireless communication for biomedical implants," *IEEE Access*, vol. 9, pp. 38 602–38 610, 2021.

[15] L. Bereuter, T. Kuenzle, T. Niederhauser, M. Kucera, D. Obrist, T. Reichlin, H. Tanner, and A. Haeberlin, "Fundamental characterization of conductive intracardiac communication for leadless multisite pacemaker systems," *IEEE Transactions on Biomedical Circuits and Systems*, vol. 13, pp. 237–247, 2 2019.

[16] M. Li, Y. Song, Y. Hou, N. Li, Y. Jiang, M. Sulaman, and Q. Hao, "Comparable investigation of characteristics for implant intra-body communication based on galvanic and capacitive coupling," *IEEE Transactions on Biomedical Circuits and Systems*, vol. 13, pp. 1747–1758, 12 2019.

[17] C. Shi, M. Song, Z. Gao, A. Bevilacqua, G. Dolmans, and Y. H. Liu, "Galvanic-coupled trans-dural data transfer for high-bandwidth intracortical neural sensing," *IEEE Transactions on Microwave Theory and Techniques*, vol. 70, pp. 4579–4589, 10 2022.

[18] S. Gabriel, R. W. Lau, and C. Gabriel, "The dielectric properties of biological tissues: iii. parametric models for the dielectric spectrum of tissues," *Phys. Med. Biol*, vol. 41, pp. 2271–2293, 1996.

[19] P. Hasgall, F. D. Gennaro, C. Baumgartner, E. Neufeld, B. Lloyd, M. Gosselin, D. Payne, A. Klingenböck, and N. Kuster. (2022) It'is database for thermal and electromagnetic parameters of biological tissues. [Online]. Available: itis.swiss/database

[20] A. Richardot and E. T. McAdams, "Harmonic analysis of low-frequency bioelectrode behavior," *IEEE Transactions on Medical Imaging*, vol. 21, pp. 604–612, 2002.

[21] ICNIRP, "Guidelines for limiting exposure to electromagnetic fields (100 khz to 300 ghz)," *Health Physics*, vol. 118, pp. 483–524, 5 2020.